

# Pressure-induced insulator-to-metal transition in low-dimensional TiOCl

C. A. Kuntscher,<sup>1\*</sup> S. Frank,<sup>1</sup> A. Pashkin,<sup>1</sup> M. Hoinkis,<sup>2,3</sup> M. Klemm,<sup>2</sup> M. Sing,<sup>3</sup> S. Horn,<sup>2</sup> and R. Claessen<sup>3</sup>

<sup>1</sup> *1. Physikalisches Institut, Universität Stuttgart, Pfaffenwaldring 57, D-70550 Stuttgart, Germany*

<sup>2</sup> *Experimentalphysik 2, Universität Augsburg, D-86135 Augsburg, Germany*

<sup>3</sup> *Experimentelle Physik 4, Universität Würzburg, D-97074 Würzburg, Germany*

(Dated: September 21, 2018)

We studied the transmittance and reflectance of the low-dimensional Mott-Hubbard insulator TiOCl in the infrared and visible frequency range as a function of pressure. The strong suppression of the transmittance and the abrupt increase of the near-infrared reflectance above 12 GPa suggest a pressure-induced insulator-to-metal transition. The pressure-dependent frequency shifts of the orbital excitations, as well as the pressure dependences of the charge gap and the spectral weight of the optical conductivity above the phase transition are presented.

Low-dimensional titanium-oxychloride, TiOCl, is under discussion recently as a spin-Peierls system with puzzling properties, like for example the occurrence of two successive phase transitions.<sup>1,2,3,4</sup> The first-order phase transition at  $T_{c1}=67$  K was attributed to a spin-Peierls transition with a dimerization of the chains of Ti atoms along the  $b$  axis.<sup>5</sup> The nature of the second-order phase transition at  $T_{c2}=91$  K is still under discussion; a transition to an incommensurate spin-Peierls state below  $T_{c2}$  with a subsequent lock-in transition to a commensurate dimerized state below  $T_{c1}$  was proposed,<sup>6,7,8</sup> but also strong orbital fluctuations with a near degeneracy of the lowest-lying orbitals were considered.<sup>2,3,4,9,10</sup>

The importance of the orbital degree of freedom in TiOCl was recently addressed by polarization-dependent transmission measurements in the infrared and visible frequency range.<sup>6,11</sup> In the transmittance spectra absorption features were observed at 0.6-0.7 eV for  $\mathbf{E}||a$  and at 1.3-1.6 eV for  $\mathbf{E}||b$ , which were interpreted in terms of excitations between the crystal field-split Ti  $3d$  energy levels. According to these results, the orbital degree of freedom is quenched due to a significant crystal field splitting of the  $t_{2g}$  orbitals. It was therefore concluded that the interesting physics of TiOCl can be entirely explained by the interplay of the lattice and spin degrees of freedom.<sup>6,11</sup>

TiOCl is a Mott-Hubbard insulator: Each Ti  $3d$  shell is occupied by one electron, and due to electronic correlations these charge carriers are localized on-site. However, the carrier localization effects should be relatively weak because of the high nearest-neighbor exchange coupling.<sup>1,3</sup> It was even suggested that TiOCl is close to an insulator-to-metal transition.<sup>1,12,13</sup> This makes the material an interesting candidate for doping, leading to a metallic and possibly superconducting state,<sup>1,13</sup> like, for example, observed in low-dimensional  $\beta\text{-Na}_{0.33}\text{V}_2\text{O}_5$  under pressure.<sup>14</sup> Unfortunately, up to now doping of TiOCl could not be achieved.

Instead of such a bandfilling control of the insulator-to-metal transition one can control the *width* of the energy bands close to the Fermi energy.<sup>15</sup> This can be accomplished by applying high external pressure. We followed this route in our study whose results we present here.

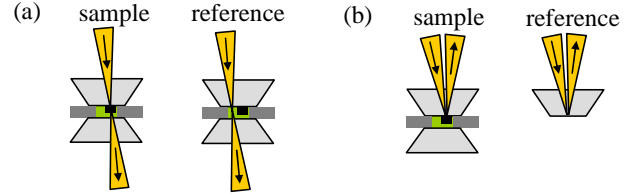


FIG. 1: (Color online) Geometry for high-pressure (a) transmittance and (b) reflectance measurements of the sample in the diamond anvil cell.

In our optical experiments on TiOCl we applied quasi-hydrostatic pressures up to 16 GPa, and indeed found large pressure-induced changes in the optical response: a strong suppression of the transmittance in the infrared and visible range and a change of the sample color from red to black. In addition, the near-infrared reflectance abruptly increases at around 12 GPa. These findings suggest the occurrence of a pressure-induced insulator-to-metal transition at 12 GPa.

The crystal structure of TiOCl consists of strongly distorted  $[\text{TiO}_4\text{Cl}_2]$  octahedra.<sup>16</sup> A different view of the structure is that of buckled Ti-O bilayers parallel to the  $ab$ -plane and separated by Cl ions. Single crystals of TiOCl were synthesized by chemical vapor transport from  $\text{TiCl}_3$  and  $\text{TiO}_2$ .<sup>16</sup> The crystal quality was validated by x-ray diffraction, specific heat, and magnetic susceptibility measurements.

A diamond anvil cell (DAC) was used for the generation of pressures up to 16 GPa. Finely ground CsI powder was chosen as quasi-hydrostatic pressure transmitting medium. For each transmittance and reflectance measurement a small piece (about  $80 \mu\text{m} \times 80 \mu\text{m}$ ) was cut from single crystals with a thickness of  $\leq 5 \mu\text{m}$  and placed in the hole of a steel gasket. The pressure was determined by the ruby luminescence method.<sup>17</sup>

Pressure-dependent transmittance and reflectance experiments were conducted at room temperature using a Bruker IFS 66v/S FT-IR spectrometer with an infrared microscope (Bruker IRscope II). The reproducibility of the results was ensured by several experimental runs on

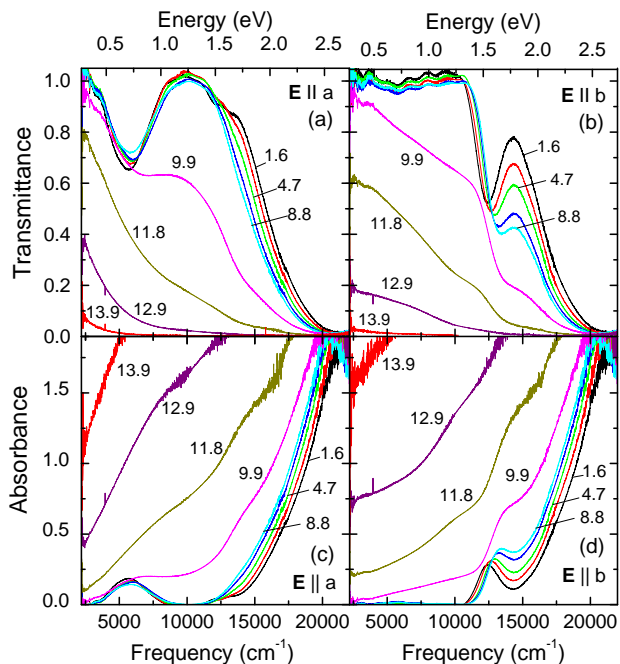


FIG. 2: (Color online) Room-temperature transmittance  $T(\omega)=I_{s-csI}(\omega)/I_{csI}(\omega)$  (see text for definitions) of TiOCl as a function of pressure for the polarization (a)  $\mathbf{E}||a$  and (b)  $\mathbf{E}||b$ . The lower graphs show the corresponding absorbance  $A=\log_{10}(1/T)$  as a function of pressure for (c)  $\mathbf{E}||a$  and (d)  $\mathbf{E}||b$ . The numbers indicate the applied pressures in GPa.

different pieces of eight crystals. For all measurements the sample was in direct contact with the diamond anvil on the upper side of the DAC, facing the incoming beam (see measurement geometry illustrated in Fig. 1). In all other directions the sample was surrounded by the pressure transmitting medium.

The pressure-dependent transmittance was studied in a wide frequency range (2000 - 22000  $\text{cm}^{-1}$ ) for the polarization directions  $\mathbf{E}||a, b$ . We measured the intensity  $I_{s-csI}(\omega)$  of the radiation transmitting the sample [see Fig. 1(a)]; as reference, for each pressure we focused the incident radiation spot on the empty space in the gasket hole next to the sample and obtained the transmitted intensity  $I_{csI}(\omega)$ . The ratio  $T(\omega)=I_{s-csI}(\omega)/I_{csI}(\omega)$  is a measure of the transmittance of the sample, and the corresponding absorbance is calculated according to  $A=\log_{10}(1/T)$ ;  $A$  is a measure of the optical conductivity.

Pressure-dependent reflectance measurements were carried out in the frequency range 2000 - 11000  $\text{cm}^{-1}$  for  $\mathbf{E}||a, b$ . Reflectance spectra,  $R_{s-d}$ , of the sample with respect to diamond were obtained by measuring the intensity  $I_{s-dia}(\omega)$  reflected at the interface between the sample and the diamond anvil [see Fig. 1(b)]. As reference, the intensity  $I_{dia}(\omega)$  reflected from the inner diamond-air interface of the empty DAC was used. The reflectance spectra were calculated according to  $R_{s-d}(\omega) = R_{dia} \cdot I_{s-dia}(\omega)/I_{dia}(\omega)$ , where  $R_{dia}$  was estimated from the refractive index of diamond  $n_{dia}$  to 0.167

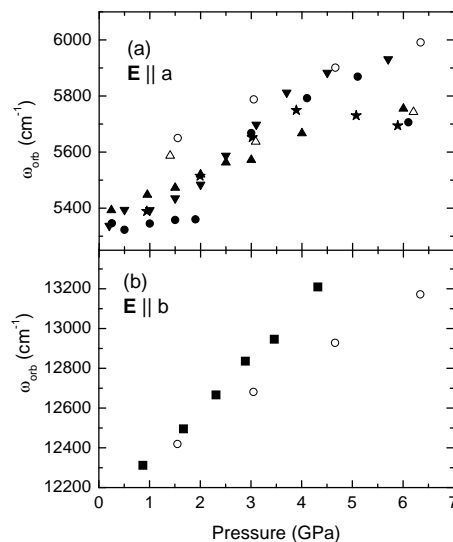


FIG. 3: Pressure-dependent positions of the orbital excitations of TiOCl, shifting to higher frequencies with increasing pressure, for (a)  $\mathbf{E}||a$  and (b)  $\mathbf{E}||b$ . Different symbols correspond to different measurements.

and assumed to be independent of pressure.<sup>18,19</sup>

The pressure-dependent transmittance and absorbance spectra of TiOCl for pressures up to 13.9 GPa are shown in Fig. 2; above 13.9 GPa the transmitted signal is zero. For the lowest applied pressure pronounced absorption features are observed at around 5300  $\text{cm}^{-1}$  (0.66 eV) and 12300  $\text{cm}^{-1}$  (1.53 eV) in the  $\mathbf{E}||a$  and  $\mathbf{E}||b$  absorbance spectra, respectively [Figs. 2(c) and 2(d)]. The two absorption features can be attributed to excitations between the Ti 3d energy levels whose degeneracy is lifted by the crystal field.<sup>6,11</sup> Since our transmittance measurements were carried out on very thin samples (thickness  $\leq 5 \mu\text{m}$ ), we could determine the precise positions and shapes of the two orbital excitations. Both absorption peaks are symmetric and can be described by a Gaussian lineshape. (For fitting the orbital excitation around 12300  $\text{cm}^{-1}$ , an exponential function describing the Urbach tail of the charge gap<sup>20</sup> was taken into account.) The broadening resulting in a Gaussian profile is ascribed to vibrational excitations accompanying the electronic transitions.<sup>21</sup>

With increasing pressure the orbital excitations broaden and continuously shift to higher frequencies with increasing pressure (see Fig. 3). The frequency shifts indicate an increasing crystal field splitting of the Ti 3d levels, which is most probably due to pressure-induced changes of the crystal structure, like modifications of the strong distortions of the  $[\text{TiO}_4\text{Cl}_2]$  octahedra. However, due to the lack of crystal structure data under pressure we can only speculate on this issue.

The steep rise of the absorbance above 16000  $\text{cm}^{-1}$  ( $\approx 2$  eV) at lowest pressure [see Figs. 2 (c) and (d)] can be attributed to excitations across the charge gap.<sup>6,11</sup> We estimated the charge gap,  $\Delta$ , by a linear extrapolation

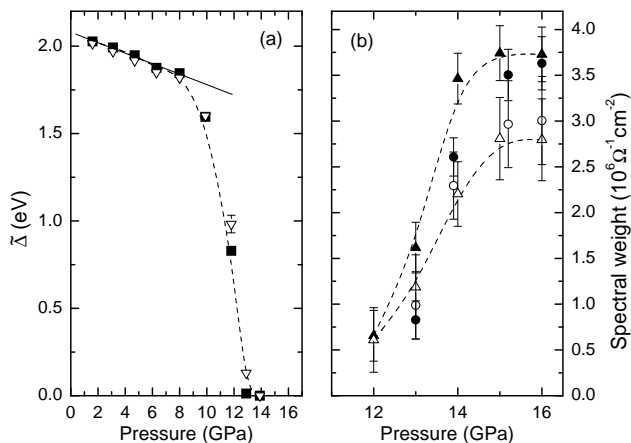


FIG. 4: (a) Charge gap  $\tilde{\Delta}$  (see text for definition) as a function of pressure for  $\mathbf{E}||a$  (full symbols) and  $\mathbf{E}||b$  (open symbols). The full line indicates a linear fit to the data; the dashed line is a guide to the eye. (b) Pressure dependence of the spectral weight of the optical conductivity above the insulator-to-metal transition. Full and open symbols correspond to  $\mathbf{E}||a$  and  $\mathbf{E}||b$ , respectively. The same symbols indicate results from the same experimental run. Dashed lines are guides to the eye.

tion (not shown) of the steep absorption edge. Starting from the lowest applied pressure,  $\tilde{\Delta}$  initially exhibits a small linear decrease of about  $240 \text{ cm}^{-1}/\text{GPa}$  [see Fig. 4(a)]. However, above 8 GPa the absorption edge rapidly shifts to lower frequencies (see also Fig. 2), indicating the abrupt closure of the charge gap. Above  $\approx 12$  GPa the  $\mathbf{E}||a, b$  transmittance is suppressed over the whole studied frequency range, and the overall absorbance is strongly enhanced at these high pressures (Fig. 2).

Associated with the rapid reduction of the charge gap is a change of the sample color. Fig. 5 depicts the view on the sample inside the DAC at different pressures: At ambient pressure the sample appears red, since only in-

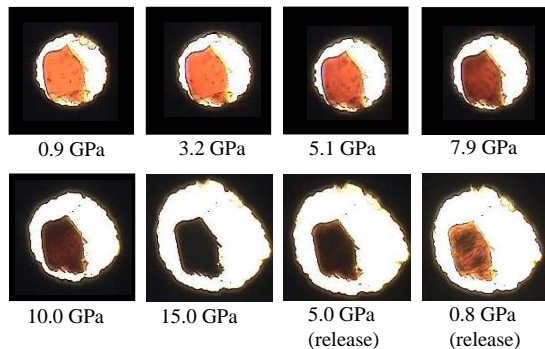


FIG. 5: (Color online) View inside the diamond anvil cell during the pressure-dependent optical measurements. With increasing pressure the sample color changes from red to black. Upon pressure release the sample does not completely recover its original color.

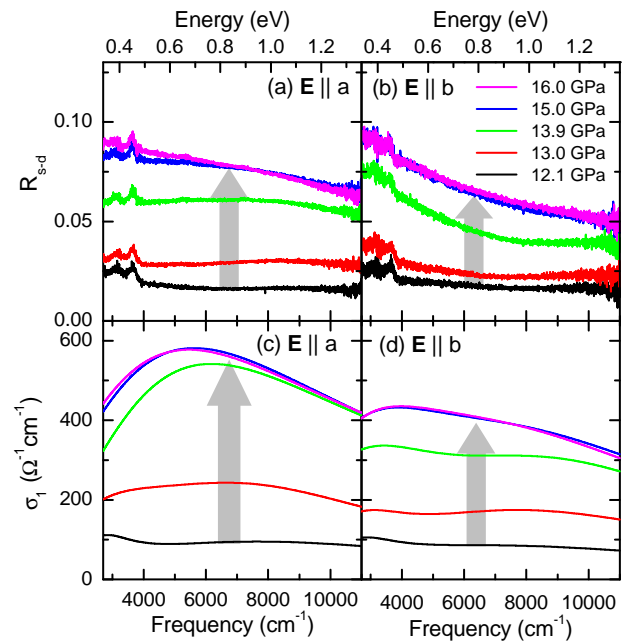


FIG. 6: (Color online) Room-temperature reflectance spectra  $R_{s-d}(\omega)$  as a function of pressure for the polarization (a)  $\mathbf{E}||a$  and (b)  $\mathbf{E}||b$ . The lower graphs show the corresponding real part  $\sigma_1(\omega)$  of the optical conductivity obtained by fitting of the  $R_{s-d}(\omega)$  data with the Drude-Lorentz model for (c)  $\mathbf{E}||a$  and (d)  $\mathbf{E}||b$ . Arrows indicate the changes with increasing pressure.

cident radiation with frequencies below the charge gap ( $\approx 2$  eV) is transmitted. Due to the strong suppression of the transmittance above  $\approx 9$  GPa, the sample color changes from red to black. Upon pressure release the sample does not completely recover its original color, as illustrated by some parts of the sample remaining black. It thus seems that the pressure-induced reduction of the charge gap is not reversible, at least in parts of the sample.

Since  $\text{TiOCl}$  becomes opaque for pressures above  $\approx 12$  GPa, we completed our spectroscopic study with pressure-dependent reflectance measurements in the near-infrared range for  $\mathbf{E}||a, b$  [see Figs. 6(a) and (b)].<sup>22</sup> For pressures below 12 GPa the reflectance  $R_{s-d}(\omega)$  is very low (about 3%); it cannot be correctly analyzed due to partial transparency of the sample, and will therefore not be considered. At around 12 GPa,  $R_{s-d}(\omega)$  abruptly increases in the whole studied frequency range for both polarization directions. We ascribe this abrupt increase to additional excitations in the infrared range induced for pressures above 12 GPa. In order to determine their contribution to the optical conductivity of the sample, we fitted the reflectance spectra with the Drude-Lorentz model,<sup>23</sup> as demonstrated in Ref. 24. The additional excitations were described by a Drude term and two Lorentz oscillators, associated with a mid-infrared peak. The appearance of these additional absorption

features is expected for a filling-controlled or thermally induced Mott transition<sup>15,25</sup> and was recently also observed in the course of a bandwidth-controlled insulator-to-metal transition,<sup>26</sup> like in the present study. The real part  $\sigma_1(\omega)$  of the optical conductivity obtained from the fitting is shown in Figs. 6(c) and (d). One clearly observes the rapid onset of a broad mid-infrared absorption band above 12 GPa for both polarizations.

To obtain a measure of the spectral weight of the pressure-induced excitations, we integrated the real part  $\sigma_1(\omega)$  of the optical conductivity between 3000 and 10000  $\text{cm}^{-1}$ . Fig. 4(b) shows the so-obtained spectral weight as a function of pressure above 12 GPa for both polarizations. It increases approximately linearly with increasing pressure and appears to saturate above  $\approx 15$  GPa. Together with the concomitant abrupt closure of the charge gap at around 12 GPa [see Fig. 4(a)], this demonstrates the transition-like character of the pressure-induced changes in the optical response. The exact determination of the spectral weight transfer from the charge gap excitations to the Drude term and mid-infrared peak requires pressure-dependent reflectance data over a broader frequency range; this will be the subject of a future study.

In conclusion, we studied the pressure dependence

of the optical response of low-dimensional insulating TiOCl in the infrared and visible frequency range at room temperature. The orbital excitations located at ambient pressure at around 0.66 and 1.53 eV for the polarizations  $\mathbf{E}||a$  and  $\mathbf{E}||b$ , respectively, broaden and shift to higher frequencies with increasing pressure. The pressure-induced frequency shifts indicate an increasing crystal field splitting of the Ti 3d energy levels suggestive for crystal structure changes. Both orbital absorption features are symmetric and have a Gaussian lineshape. With increasing pressure, a strong suppression of the transmittance in the infrared and visible energy range and a change of the sample color are observed. We attribute these effects to a rapid reduction of the charge gap. At  $\approx 12$  GPa the near-infrared reflectance spectra for both studied polarizations abruptly increase. This is attributed to additional excitations in the infrared frequency range, which can be described by a Drude term and a mid-infrared absorption band. All these findings suggest a pressure-induced insulator-to-metal transition in TiOCl at around 12 GPa.

We thank M. Dressel for stimulating discussions. Financial support by the DFG through the Emmy Noether program and SFB 484 is acknowledged.

- 
- \* Email: kuntscher@pi1.physik.uni-stuttgart.de
- 1 A. Seidel, C. A. Marianetti, F. C. Chou, B. Ceder, and P. A. Lee, *Phys. Rev. B* **67**, 020405 (2003).
  - 2 T. Imai and F. C. Chou, *cond-mat/0301425* (unpublished).
  - 3 V. Kataev, J. Baier, A. Möller, L. Jongen, G. Meyer, and A. Freimuth, *Phys. Rev. B* **68**, 140405 (R) (2003).
  - 4 J. Hemberger, M. Hoinkis, M. Klemm, M. Sing, R. Claessen, S. Horn, and A. Loidl, *Phys. Rev. B* **72**, 012420 (2005).
  - 5 M. Shaz, S. van Smaalen, L. Palatinus, M. Hoinkis, M. Klemm, S. Horn, and R. Claessen, *Phys. Rev. B* **71**, 100405 (2005).
  - 6 R. Rückamp, J. Baier, M. Kriener, M. W. Haverkort, T. Lorenz, G. S. Uhrig, L. Jongen, A. Möller, G. Meyer, and M. Grüninger, *Phys. Rev. Lett.* **95**, 097203 (2005).
  - 7 A. Krimmel et al. (unpublished).
  - 8 S. van Smaalen, L. Palatinus, and A. Schönleber, *Phys. Rev. B* **72**, 020105(R) (2005).
  - 9 T. Saha-Dasgupta, R. Valentí, H. Rosner, and C. Gros, *Europhys. Lett.* **67**, 63 (2004).
  - 10 P. Lemmens, K. Y. Choi, G. Caimi, L. Degiorgi, N. N. Kovaleva, A. Seidel, and F. C. Chou, *Phys. Rev. B* **70**, 134429 (2004).
  - 11 R. Rückamp, E. Benckiser, M. W. Haverkort, H. Roth, T. Lorenz, A. Freimuth, L. Jongen, A. Möller, G. Meyer, P. Reutler, B. Büchner, A. Revcolevschi, S.-W. Cheong, C. Sekar, G. Krabbes, and M. Grüninger, *New J. Phys.* **7**, 144 (2005).
  - 12 R. J. Beynon and J. A. Wilson, *J. Phys.: Condens. Matter* **5**, 1983 (1993).
  - 13 L. Craco, M. S. Laad, and E. Müller-Hartmann, *cond-mat/0410472*.
  - 14 T. Yamauchi, Y. Ueda, and N. Môri, *Phys. Rev. Lett.* **89**, 057002 (2002).
  - 15 M. Imada, A. Fujimori, and Y. Tokura, *Rev. Mod. Phys.* **70**, 1039 (1998).
  - 16 H. Schäfer, F. Wartenpfehl, and E. Weise, *Z. Anorg. Allg. Chem.* **295**, 268 (1958).
  - 17 H. K. Mao, J. Xu, and P. M. Bell, *J. Geophys. Res. [Atmos.]* **91**, 4673 (1986).
  - 18 M. I. Eremets and Y. A. Timofeev, *Rev. Scient. Instrum.* **63**, 3123 (1992).
  - 19 A. L. Ruoff and K. Ghandehari, in S. C. Schmidt, J. W. Shaner, G. A. Samara, and M. Ross (Eds.), *High Pressure Science and Technology*, pp. 1523-1525, American Institute of Physics Conference Proceedings 309, Woodbury, N.Y. (1994).
  - 20 F. Urbach, *Phys. Rev.* **92**, 1324 (1953).
  - 21 B. N. Figgis and M. A. Hitchman, *Ligand field theory and its applications*, Wiley-VCH, New York (1996).
  - 22 The features around 3200 and 3600  $\text{cm}^{-1}$  are artifacts due to multiphonon absorption by diamond and no intrinsic properties of the studied sample.
  - 23 The background dielectric constant  $\epsilon_\infty=3.7$  was determined by a Drude-Lorentz fit of ambient-pressure reflectivity data measured on a free-standing thick sample and assumed to be pressure-independent.
  - 24 C. A. Kuntscher, S. Frank, I. Loa, K. Syassen, T. Yamauchi, and Y. Ueda, *Phys. Rev. B* **71**, 220502(R) (2005).
  - 25 M. J. Rozenberg, G. Kotliar, and H. Kajueter, *Phys. Rev. B* **54**, 8452 (1996).
  - 26 I. Kézsmérki, N. Hanasaki, D. Hashimoto, S. Iguchi, Y. Taguchi, S. Miyasaka, and Y. Tokura, *Phys. Rev. Lett.* **93**, 266401 (2004).